processes

MDPI

Article

Low-Carbon Economy Optimization of Park-Level Integrated Energy Systems Considering Temporal and Spatial Scheduling of Large-Scale Electric Vehicles

Yudong Wang [1,*], Huijuan Huo [1], Shuo Wang [1], Tianqiong Chen [1], Weiwei Li [1], Rui Zhao [2], Cheng Xin [1], Jing Duan [1], Bingkang Li [3] and Nianduo Li [3]

[1] State Grid Economic and Technological Research Institute Co., Ltd., Beijing 102209, China
[2] Economic and Technical Research Institute, State Grid Ningxia Electric Power Co., Ltd., Ningxia 750011, China
[3] Department of Economic Management, North China Electric Power University, Baoding 071003, China
* Correspondence: wyd18813151725@163.com

Abstract

Park-level integrated energy systems (PIESs) realize coordinated carbon reduction via multi-energy coupling and multi-agent flexibility, yet few studies jointly optimize the temporal and spatial scheduling of large fleets of electric vehicles (EVs) for low-carbon economic dispatch. This paper develops a bi-layer scheduling model for PIESs integrated with large EV fleets. The upper layer adopts multi-objective optimization to minimize operating costs and maximize carbon abatement, coordinating CHP, boilers, energy storage, PV and aggregate EV power across a 24 h horizon. A carbon emission intensity index (CEI) is defined to trace embodied carbon flows and impose system carbon constraints. The lower layer minimizes distribution network power loss by rationally assigning EV charging/discharging loads to network nodes subject to voltage, line capacity and charging pile limits. NSGA-II with fuzzy decision-making solves the upper multi-objective MINLP, and Gurobi addresses the lower MILP power flow model. Simulations on a modified IEEE 33-node park system with four comparative cases validate the proposed strategy. Results show that, compared with disordered EV charging, the bi-layer scheme cuts total cost by 18.2%, net carbon emissions by 42.1% and network losses by 17.4%. Sensitivity analysis proves that the carbon price and EV penetration remarkably affect economic and low-carbon performance. This two-stage spatio-temporal optimization framework provides an effective tool to harness the low-carbon flexibility potential of large-scale EV fleets in industrial and commercial parks.

Keywords: park integrated energy system; large-scale electric vehicles; spatio-temporal scheduling; bi-layer optimization; low-carbon economic dispatch

Check for updates

Academic Editor: Paulraj Arunkumar

Received: 13 August 2026
Revised: 13 October 2026
Accepted: 14 October 2026
Published: 2 November 2026

Copyright: © 2026 by the authors. Licensee MDPI, Basel, Switzerland. This article is an open access article distributed under the terms and conditions of the Creative Commons Attribution (CC BY) license.

1. Introduction

Amid growing environmental concerns, park-level integrated energy systems (PIESs) have drawn increasing scholarly attention as a promising pathway to enhance energy efficiency and reduce carbon emissions [1]. In the face of continued global climate deterioration, China has set more ambitious decarbonization targets, pledging to peak carbon emissions by 2030 and achieve carbon neutrality by 2060 [2]. Against this stringent policy backdrop, reconciling system operational efficiency with both economic viability and environmental sustainability has emerged as a critical research priority.

With the rapid growth of EV ownership, large numbers of electric vehicles are widely parked within industrial–commercial parks. Uncoordinated EV charging and discharging

behaviors pose tangible risks to real-world PIES operation: uncontrolled EV loads increase overall operating expenditures, raise carbon emissions, induce local node-voltage deviations and aggravate distribution network power losses. Although the existing literature has investigated low-carbon dispatch for integrated energy systems and flexible EV scheduling separately, few studies address the joint spatio-temporal management of large-scale EV fleets in park-level multi-energy coupling scenarios. This creates a practical research challenge: how to make full use of EV flexibility while jointly satisfying economic, decarbonization and distribution network security requirements.

Substantial efforts have been devoted to low-carbon economic optimization of integrated energy systems (IESs), spanning multiple methodological perspectives including carbon trading mechanisms, carbon conversion technologies, demand-side management (DSM), and low-carbon dispatch strategies. Since the pilot launch of carbon trading in seven Chinese cities in late 2011, new policy instruments have become available for IES emission mitigation. For instance, ref. [3] developed a two-stage scheduling model to examine the environmental benefits of consumer participation in both electricity and carbon emission trading markets through proactive DSM. Ref. [4] proposed a low-carbon-oriented optimal dispatch approach for coupled natural gas and electricity systems incorporating carbon emission trading, while ref. [5] formulated and compared global and partition-based dynamic power dispatch problems with wind power integration under a carbon trading framework. Ref. [6] constructed a model that coordinates demand-side resources—including electric vehicles, demand response, and distributed generation—while capturing the influence of carbon trading on generation scheduling. Ref. [7] investigated bidding strategies for virtual power plants participating in integrated carbon–electricity trading within ancillary service markets. Beyond carbon trading, DSM has also proven effective in curbing IES emissions. Ref. [8] assessed the low-carbon contributions of industrial demand response for ancillary service provision; ref. [9] analyzed the joint effects of demand response aggregators and carbon taxation on power system emission reductions; ref. [10] developed a resident behavior detection model for environmentally responsive demand response aimed at mitigating CO_2 emissions; ref. [11] employed multi-objective dynamic optimal power flow to examine day-ahead scheduling of power systems with wind generation and demand response; and ref. [12] introduced a novel emission reduction mechanism that incentivizes active user participation to lower power system carbon output.

Complementary strands of research have investigated IES decarbonization through carbon capture and conversion pathways. Ref. [13] proposed an original analytical framework to evaluate diverse power-to-gas processes and their operational implications for carbon reduction in electricity and gas transmission networks. Ref. [14] examined the operational envelope and optimal scheduling of combined power-to-gas and gas-fired systems to quantify their capacity for emission abatement and renewable integration. Ref. [15] developed a source–load-coordinated low-carbon economic dispatch model to address insufficient carbon capture during peak-load periods within the low-carbon retrofitting of thermal power units. In conjunction with these strategies, synergistic optimization of flexible IES components, such as combined heat and power (CHP) units, electric boilers (EBs), energy storage (ES), and adjustable loads, has been identified as a key enabler of low-carbon economic operation. Ref. [16] proposed a bi-level optimal dispatch model for industrial parks to coordinate energy conversion equipment operation and set rational energy prices. Ref. [17] presented a low-carbon dispatch model for electricity–gas systems, examining the differential impacts of various low-carbon technologies on system economy and emissions. Ref. [18] introduced a two-stage low-carbon scheduling framework integrating carbon emission flow theory and price-based demand response. Ref. [19] explored multi-energy

system low-carbon operation through energy-carbon integrated pricing coordinated across transmission and distribution levels.

Given the rapid proliferation of electric vehicles (EVs) and their inherent schedulable flexibility, utilizing EVs as controllable loads for peak shaving and demand response offers substantial potential for improving IES energy efficiency. Ref. [20] devised optimal home energy management strategies incorporating solar power, storage, and vehicle-to-grid capabilities under predefined demand response scenarios. Ref. [21] tackled energy scheduling challenges in office buildings with integrated photovoltaics and workplace EV charging, leveraging day-ahead electricity markets and time-of-use pricing. Ref. [22] proposed a carbon-oriented expansion planning model for integrated electricity–gas systems with EV fast-charging stations to ensure planning scheme carbon performance. Ref. [23] developed a two-stage energy exchange scheduling strategy for multi-microgrid systems, treating EVs as storage assets to moderate power exchange peaks with the main grid. Ref. [24] presented a day-ahead optimal scheduling framework for virtual power plants enabling zero-carbon multi-energy dispatch and multi-flexible EV potential, while accounting for uncertainties across diverse scenarios. Ref. [25] introduced a robust optimization method for energy hubs integrating thermal and electrical demand response under varying EV charging modes.

Collectively, these studies have yielded notable advances in low-carbon IES operations and, in some instances, incorporated EVs as flexible resources. Looking ahead, as PIESs continue to expand, an increasing number of EVs will be distributed across residential, office, and commercial zones within park settings. If such EVs are leveraged as mobile energy storage units, they could substantially augment the adjustable resource pool for PIES low-carbon dispatch and enhance carbon emission adjustment flexibility. Nevertheless, few existing studies have explicitly treated large-scale EV fleets as flexible resources in PIES low-carbon economic optimization.

With the continuous deployment of V2G charging pile pilot projects for industrial and commercial parks in China, large-scale EVs possess basic hardware conditions to provide bidirectional regulation services for park-level integrated energy systems. However, practical V2G operation still faces realistic constraints, such as insufficient user-participation willingness and imperfect battery-degradation-compensation mechanisms. This paper carries out scheduling optimization under the premise of reasonable economic incentives, which is consistent with the current application scenarios of park V2G pilot projects. The proposed bi-layer scheduling framework can provide effective operational decision support for real-world park energy management.

To further highlight the research gaps and innovations of this work against the existing literature, a qualitative comparison table is presented in Appendix A. Representative published papers covering park-level-integrated-energy-system dispatch and EV flexible scheduling are compared in terms of research object, EV spatio-temporal co-optimization capability, model architecture, low-carbon indicators, solving approaches and test platforms.

Against the above-mentioned research limitations, this paper develops a bi-layer spatio-temporal collaborative optimization framework for PIESs with massive EV fleets. The upper layer conducts multi-objective day-ahead multi-dispatch with the proposed carbon emission intensity (CEI) index, and the lower layer optimizes spatial EV-load allocation to mitigate network losses. This framework enables coordinated temporal power scheduling and spatial node-level load distribution of EVs and provides decision support for park-energy operators. The main contributions of this work are summarized as follows:

(1) A bi-layer decoupled optimization architecture is proposed to separate EV temporal power scheduling and spatial load allocation. The upper layer conducts system-level multi-energy day-ahead dispatch from the time dimension, while the lower layer realizes EV-load spatial distribution based on optimal power flow, which organically

combines multi-energy low-carbon economic operation and distribution network-loss reduction.

(2) A carbon emission intensity index (CEI) derived from carbon emission flow theory is introduced to quantify implicit carbon flows of electricity and heat supply. Corresponding carbon-balance constraints are formulated to realize unified carbon measurement and emission control for the whole PIES.

(3) A combined solving strategy of NSGA-II with fuzzy membership decision-making and the Gurobi solver is adopted. The upper-layer multi-objective mixed integer nonlinear-programming model and lower-layer mixed integer linear power flow model are solved efficiently to balance system economy and carbon reduction performance.

(4) Multiple comparative scenarios and sensitivity analysis are carried out on a modified IEEE 33-node park test system. Simulation results verify that the proposed bi-layer scheduling method can fully tap the flexible low-carbon potential of large-scale EVs, significantly cutting operating costs, net carbon emissions and distribution network-power losses simultaneously.

While this study adopts several well-established basic theories from the existing literature, including carbon emission flow theory, optimal power flow formulation, and fuzzy decision-making methods, all core innovations claimed in this paper are fully demonstrated and validated in subsequent chapters. Specifically, the proposed bi-layer decoupled scheduling architecture is elaborated with complete mathematical constraints and verified through spatial–temporal collaborative scheduling results. The customized CEI low-carbon quantification mechanism is comprehensively explained and numerically validated through carbon flow distribution analysis. The hybrid multi-objective solution strategy is benchmarked against classical algorithms to verify its superiority in efficiency and stability. Meanwhile, multiple quantitative evaluation metrics, including operating cost, carbon emission, network loss, and algorithm performance indicators, are clearly defined and consistently adopted throughout the case studies to comprehensively evaluate the economic, low-carbon, and operational performance of the proposed framework.

The rest of this paper is organized as follows. Section 2 illustrates the system configuration and bi-layer spatio-temporal scheduling framework. Section 3 establishes the mathematical optimization model and solution strategy. Section 4 conducts scenario simulation, result analysis and multi-dimensional supplementary verification. Section 5 summarizes the core conclusions and proposes future research directions.

2. System Structure and Optimization Framework

2.1. System Architecture of the PIES

The PIES studied in this paper is the energy supplier of end users, and it is the link between users and urban energy system. The PIES includes the electricity sub-system, gas sub-system and thermal sub-system. Figure 1 is a typical system structure of the PIES.

The electricity sub-system in PIESs consists of EH and distribution network (10 kV). EH is the direct provider of user electricity demand and EV electricity demand in distribution network. The EH is also interconnected with high-voltage power grid (110 kV). The thermal sub-system in PIESs consists of EH and thermal energy supply pipeline, and EH is the only thermal source in PIESs. The gas sub-system in PIESs can only maintain normal operation with the help of gas grid.

This paper realizes the decoupling and collaborative optimization of temporal and spatial dimensions for EV scheduling. Specifically, the upper temporal optimization focuses on the system-level energy scheduling, which determines the daily dynamic aggregate charging and discharging power curve of the EV fleet based on time-of-use electricity prices, carbon intensity and load demand. The lower spatial optimization takes the fixed aggregate

EV power output of each time period as invariant input, and only optimizes the power allocation of EVs at different distribution network nodes. The temporal dimension determines the total energy regulation volume and system-level economic-low carbon performance, while the spatial dimension optimizes the distribution network power flow and voltage safety. The collaborative coupling of the two dimensions realizes the comprehensive optimization of energy economy, low-carbon performance and network operation safety.

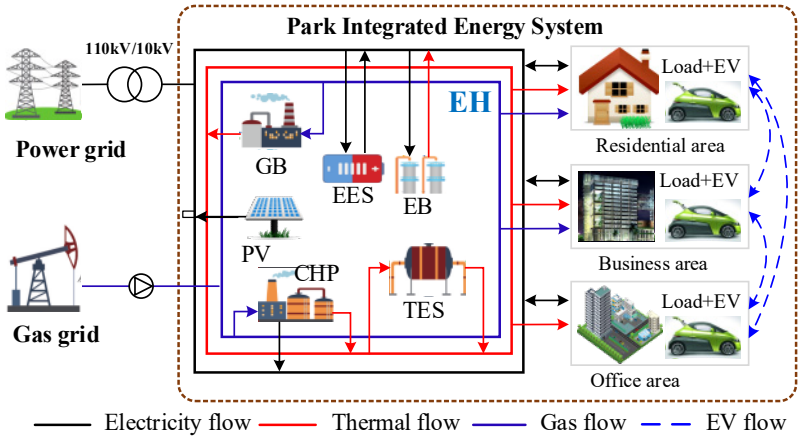


Figure 1. Typical system structure of integrated energy system.

2.2. Bi-Layer Optimization Framework of PIES

The proposed bi-layer optimization method, shown in Figure 2, consists of upper layer optimization for PIES and lower layer optimization for distribution network.

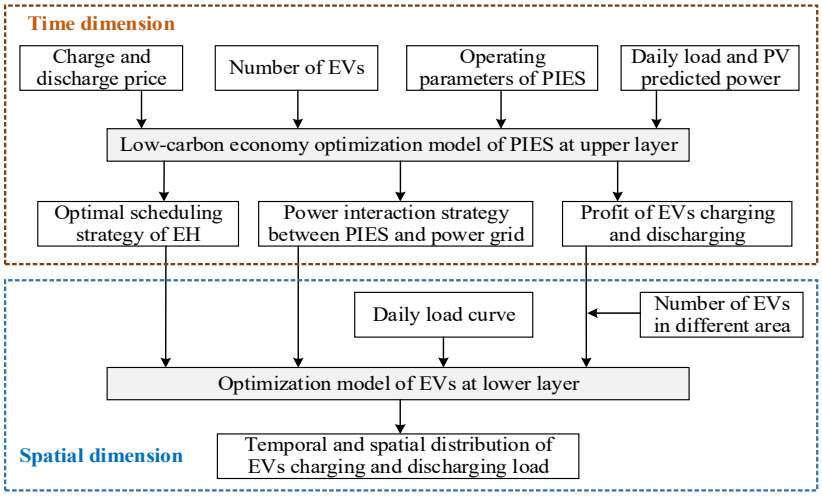


Figure 2. The structure of the bi-layer optimization.

On the PIES optimization level, the upper layer time-domain optimization model considering economic operation and carbon emission reduction coordinates the charging and/or discharge schedule of EVs with EH, power grid, and load. The charging and discharging behaviors of EVs are optimized from temporal dimension. On the distribution network optimization level, the lower-layer spatial-domain optimization model considering power losses solves optimal load location for EVs. It can figure out where EVs should be charged or discharged. The charging and discharging behaviors of EVs are optimized from spatial dimension. The number of EVs charging and discharging obtained from the optimization of the upper layer model will be used as the basic parameter of the optimization of the lower-layer model.

3. Bi-Level Optimization Model

3.1. Operational Optimization Model at Upper Layer

From a view of system, the upper layer optimization dispatches units of EH and EVs to obtain better economic performance on EH operation and power grid dispatching. A day-ahead model is proposed in the upper layer to coordinate EH units and EVs to minimize the cost while meeting the load demand.

3.1.1. Objective Function

The objective function mainly considers the economy of operation and carbon emission reduction.

(1) Economic objective function

The economic objective function to reduce the operating costs of units, charging costs of users, and power interaction cost with grid can be described as follows.

$$F_1 = min\sum_{t=1}^{T}\left(C_t^{gas} + C_t^{grid} + C_t^{op} + C_t^{EVs}\right) \tag{1}$$

$$C_t^{gas} = \frac{c^{gas}P_{chp,t}}{\eta_{chp} \times LHV_{NG}}\Delta t + \frac{c^{gas}P_{gb,t}}{\eta_{gb} \times LHV_{NG}}\Delta t \tag{2}$$

$$C_t^{gas} = \frac{c^{gas}P_{chp,t}}{\eta_{chp} \times LHV_{NG}}\Delta t + \frac{c^{gas}P_{gb,t}}{\eta_{gb} \times LHV_{NG}}\Delta t \tag{3}$$

$$C_t^{op} = \sum_{k=1}^{K} c_{k,t}^{op}P_{k,t}\Delta t \tag{4}$$

The charging cost of users represents the financial cost of all EV users, calculated by charging cost minus discharging income.

$$C_t^{EVs} = N_{cha,t}c_{cha,t}^{ele}P_{cha,t}^{EV}\Delta t - N_{dis,t}c_{dis,t}^{ele}P_{dis,t}^{EV}\Delta t \tag{5}$$

(2) Carbon emissions reduction objective

The carbon emissions reduction objective is modeled as Equation (6). The carbon emission reduction is defined by the difference between the total carbon emission and the total carbon quota.

$$F_2 = max\sum_{t=1}^{T}\left(E_t^q - E_t^e\right)\Delta t \tag{6}$$

where E_t^e is the total carbon emissions; E_t^q is the total carbon quota.

This paper defines the CEI index to reflect the actual carbon emissions in PIESs. Based on the carbon emission flow theory and the proportional sharing assumption theory [8,14], the CEI index is proposed to reflect the carbon emission intensity of power grid and EH. The CEI index represents the average carbon emission related to the injected energy flow during a certain time period, which is equal to the weighted average of carbon intensities of all the injected energy flows.

Since the CEI index in the IES has considered different carbon emission inflows, the carbon emission in the IES is defined by the product of CEI index and load. The carbon quota in IES is distributed according to the electricity supply and thermal supply capacity of CHP and GB.

$$E_t^e = \rho_{EH,t}^e\left(P_{el,t} + P_{cha,t}^{EV} - P_{dis,t}^{EV}\right)\Delta t + \rho_{EH,t}^t P_{tl,t}\Delta t \tag{7}$$

$$E_t^q = q_{gas}^e P_{chp}^{cap} + q_{gas}^t \mu_{chp} P_{chp}^{cap} + q_{gas}^t P_{gb}^{cap} \tag{8}$$

Equation (9) defines electrical CEI index of power grid, Equations (10) and (11) define the electrical CEI index and thermal CEI index of EH, and Equations (12) and (13) define the CEI index of CHP and GB.

The carbon emission in the power grid mainly comes from coal-fired units and the carbon input from IES.

$$\rho^{e}_{grid,t} = \frac{\rho^{e}_{coal,t}P^{+}_{grid,t} + \rho^{e}_{EH,t}P^{-}_{grid,t}}{P^{+}_{grid,t} + P^{-}_{grid,t}}\Delta t \tag{9}$$

In particular, $P^{+}_{grid,t}P^{-}_{grid,t} = 0$, and when $P^{+}_{grid,t} = P^{-}_{grid,t} = 0$, $\rho^{e}_{grid,t} = 0$.

The carbon accompanying electricity in EH mainly comes from CHP and carbon input from power grid [1,11,19]. The carbon accompanying thermal energy in EH mainly comes from CHP and GB.

$$\rho^{e}_{EH,t} = \frac{\rho^{e}_{grid,t}P^{+}_{grid,t} + \left(1+\mu_{chp}\right)^{-1}\rho^{e}_{chp,t}P_{chp,t}}{P^{+}_{grid,t} + P_{chp,t} + P_{pv,t}}\Delta t \tag{10}$$

$$\rho^{t}_{EH,t} = \frac{\rho^{e}_{gb,t}P_{gb,t} + \left[1-\left(1+\mu_{chp}\right)^{-1}\right]\rho^{e}_{chp,t}P_{chp,t}}{\mu_{chp}P_{chp,t} + P_{gb,t}}\Delta t \tag{11}$$

$$\rho^{e}_{chp,t} = \frac{P_{chp,t}}{\eta_{chp} \times LHV_{NG}} \tag{12}$$

$$\rho^{e}_{gb,t} = \frac{P_{gb,t}}{\eta_{gb} \times LHV_{NG}} \tag{13}$$

where $\rho^{e}_{EH,t}$ is the electrical CEI index of the EH, kg/kWh; $\rho^{t}_{EH,t}$ is the thermal CEI index of EH, kg/kWh; $\rho^{e}_{grid,t}$ is the electrical CEI index of the power grid, kg/kWh.

3.1.2. Constraints

(1) Power balance constraint

The power balance constraints of electricity sub-system and thermal sub-system are as follows.

$$P_{chp,t} + P_{pv,t} + P^{ees}_{dis,t} + P^{EV}_{dis,t} + P^{+}_{grid,t} - P^{EV}_{dis,t} - P^{ees}_{cha,t} - P_{eb,t} - P^{-}_{grid,t} - P_{el,t} = 0 \tag{14}$$

$$\mu_{chp}P_{chp,t} + P_{gb,t} + P^{tes}_{dis,t} + \mu_{eb}P_{eb,t} - P^{tes}_{cha,t} - P_{tl,t} = 0 \tag{15}$$

(2) Ramp rate constraint

For each unit, the difference in output power in two adjacent time intervals is limited by ramp up/down rate. It can be represented as Equation (16).

$$P^{d}_{k} \le P_{k,t} - P_{k,t-1} \le P^{u}_{k} \tag{16}$$

(3) EV charging/discharging constraint [12,20,21]

At each time interval, the number of available EVs for charging or discharging is limited by Equation (17).

$$N_{cha,t} \le N^{max}_{cha,t}, N_{dis,t} \le N^{max}_{dis,t} \tag{17}$$

EVs require sufficient time for charging, but the discharging time has to be restricted so that EVs can retain enough energy to meet the owner's traveling need in the future. The total EVs charging or discharging duration should be constrained.

$$\sum_{t=1}^{T} N_{cha,t}\Delta t \le N^{max}_{cha,t}\Delta t, \sum_{t=1}^{T} N_{dis,t}\Delta t \le N^{max}_{dis,t}\Delta t \tag{18}$$

(4) Carbon emission constraint

The carbon emission generated during the operation of PIES cannot exceed the carbon quota. Equation (19) is the carbon emission constraint of PIES.

$$E_t^q - E_t^e \geq 0 \tag{19}$$

3.2. Optimization Model of EV at Lower Layer

3.2.1. Objective Function

With the optimization results of the number of EVs charging and discharging at time interval t obtained from the upper layer, the objective of the lower layer optimization is to minimize the power losses of distribution network by arranging EVs to charge and discharge in the optimal location of the distribution network in the PIES. The corresponding objective function can be defined as follows.

$$F = min \sum_{t=1}^{T} P_{loss,t} \Delta t \tag{20}$$

where $P_{loss,t}$ is the total network loss of distribution network at time interval t.

3.2.2. Constraints

(1) Active and reactive power balance

The active and reactive power balance must be satisfied at each node according to Kirchhoff's theory [26].

$$\begin{cases} P_{i,S,t} + N_{i,dis,t} P_{dis,t}^{EV} - P_{i,el,t} - N_{i,cha,t} P_{cha,t}^{EV} - P_{i,T,t} = 0 \\ Q_{i,S,t} - Q_{i,el,t} - Q_{i,T,t} = 0 \end{cases} \tag{21}$$

where I is the set of all nodes except the slack node, $P_{i,S,t}$ and $Q_{i,S,t}$ are the active power source and reactive power source of node i at time interval t, respectively. $P_{i,el,t}$ and $Q_{i,el,t}$ are the active and reactive power load of node a at time interval t, respectively. $N_{i,cha,t}$ and $N_{i,dis,t}$ are the number of EVs charging and discharging in node a at time interval t, respectively. $P_{i,T,t}$ and $Q_{i,T,t}$ are the transmitted active and reactive power of node a at time interval t, respectively.

(2) Node voltage constraints

In order to ensure power quality and grid security, upper and lower limits of node voltage can be denoted as Equation (22).

$$V_{i,min} \leq V_{i,t} \leq V_{i,max} \tag{22}$$

where $V_{i,max}$ and $V_{i,min}$ are the upper and lower limits of node voltage.

(3) Line capacity constraints

Transmission capacity of lines is limited by Equation (23).

$$|P_{ij,t}| \leq P_{ij,max}, \forall i,j \epsilon I \tag{23}$$

where $P_{ij,max}$ is the maximal transmission capacity of line *i-j*; $P_{ij,t}$ is the power flow on transmission line *i-j*.

(4) EV constraint

There is a certain number of charging piles in each node and so the maximal number of EVs connected to the grid is limited by Equation (24).

$$0 \leq N_{cha,i,t}, N_{dis,i,t} \leq N_{i,max} \tag{24}$$

where $N_{i,max}$ is the number of charging piles in node i.

The number of EVs in each area is changing due to their mobility. The number of EVs available for charging and discharging in a certain area can be formulated by Equation (25).

$$\sum_{i \epsilon a} N_{cha,i,t} = N_{cha,a,t}, \sum_{i \epsilon a} N_{dis,i,t} = N_{dis,a,t} \tag{25}$$

where $N_{cha,a,t}$ and $N_{dis,a,t}$ are the number of EVs available for charging and discharging in area a at time interval t.

3.3. Model Solving Method

The optimization model at the upper level is a typical multi-objective optimization problem, and involves many nonlinear, discrete, random and uncertain factors. The economic objective function and carbon emission reduction objective function restrict each other. And the optimization results include the output power of each unit in EH and the total number of EVs charging and discharging at each time interval. In this paper, the multi-objective process synthesis can be attributed to the solution of multi-objective mixed integer nonlinear programming [27] (MOMINLP). The general form of the MOMINLP problem is expressed as follows.

$$\begin{cases} \min F = \min([F_1(x,y), F_2(x,y), \ldots F_n(x,y)]) \\ J(x,y) \leq 0, H(x,y) \leq 0 \end{cases} \tag{26}$$

where x,y are the optimization variables; $F_n(x,y)$ is the optimization target; $J(x,y)$ is a set of inequality constraints; $H(x,y)$ is a set of equality constraints.

In the optimization model established in this paper, the main variables are optimization time X_t, the output power X_P of each unit, the number of EVs X_N. The set of variables is as shown in Equation (27). Table 1 shows the variable identification in the MOMINLP model presented in this paper.

$$\begin{cases} X_t = [t] \\ X_P = \left[P_{chp,t}, P_{pv,t}, P^{ees}_{dis,t}, P^{+}_{grid,t}, P^{EV}_{dis,t}, P^{ees}_{cha,t}, P^{-}_{grid,t}\right. \\ X_N = \left[N_{cha,t}, N_{dis,t}\right] \end{cases} \tag{27}$$

Table 1. Variable identification in the MOMINLP model.

	Non-negativity	Yes	No
Variables	Integer	t,$N_{cha,t}$,$N_{dis,t}$	-
	Non-integer	$P_{chp,t}$,$P_{pv,t}$, $P^{ees}_{cha,t}$, $P^{+}_{grid,t}$, $P^{EV}_{cha,t}$	$P^{ees}_{dis,t}$, $P_{eb,t}$, $P^{-}_{grid,t}$, $P^{EV}_{dis,t}$

As shown in Table 1, there are many variables in the optimization model at the upper level, and the objective function is more complex, so it is not suitable for solving the problem with multi-objective mathematical programming. The non-dominated sorting genetic algorithm II (NSGA-II) is used to solve the model in this paper [28,29]. The NSGA-II algorithm can effectively solve this problem because of its strong variable processing ability, which maintains the independence between optimization objectives to the greatest extent and better global optimization ability. The flow chart of the NSGA-II proposed is shown in Figure 3.

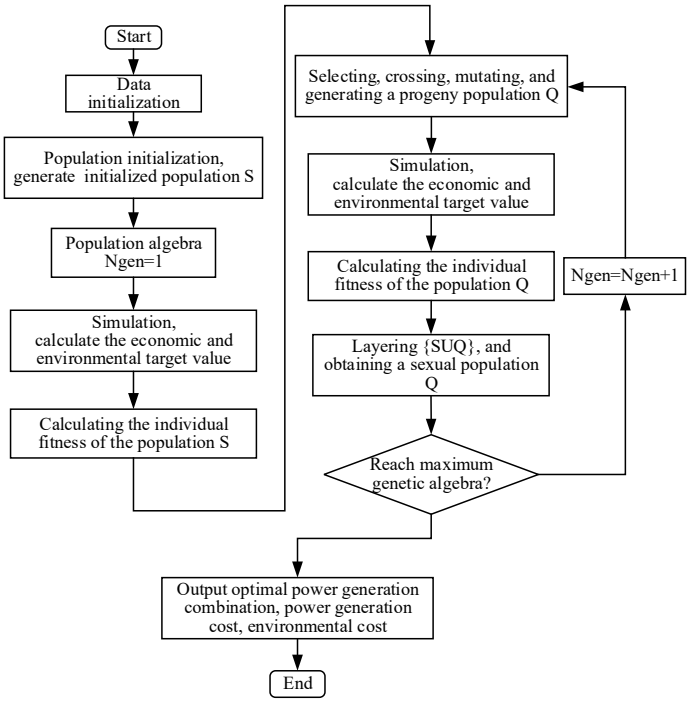


Figure 3. Flow chart of the NSGA-II.

The optimized Pareto solution set can be obtained by the NSGA-II algorithm. In order to select the optimal solution from the optimal solution set, the fuzzy membership function is used here [30]. The degree of satisfaction of decision makers with this objective optimization is reflected by the size of the membership degree, and the optimal solution is obtained by synthesizing the fuzzy membership degree of each objective function. First, the membership degree of the objective function in the Pareto solution set is calculated by Equation (28).

$$\mu_m^k = \begin{cases} 1, & F_m = F_m^{min} \\ \frac{F_m^{max} - F_m}{F_m^{max} - F_m^{min}}, & F_m^{min} \le F_m \le F_m^{max} \\ 0, & F_m = F_m^{max} \end{cases} \tag{28}$$

where F_m is the function value of the function m; F_m^{min}, F_m^{max} are the minimum and maximum values of the objective function, respectively; μ_m^k is the membership degree of the k-th Pareto solution for the m-th objective.

Then, weight coefficients are assigned according to the preference of the decision-maker, and the normalized relative satisfaction degree of each multi-objective Pareto solution is computed. The Pareto solution corresponding to the maximum normalized relative satisfaction degree is selected as the optimal compromise solution. In this work, equal weights are assigned for different objectives, and the calculation expression is given as Equation (29):

$$\mu^k = \frac{\sum_{m=1}^{N_{obj}} \lambda_m \mu_m^k}{\sum_{k=1}^{N_p} \sum_{m=1}^{N_{obj}} \lambda_m \mu_m^k} \tag{29}$$

where N_p is the population number; λ_m is the weight of the target function$i$; N_{obj} is the number of objective functions; μ^k is the normalized relative satisfaction degree of k-th Pareto solution for the m-th objective.

By linearizing the lower-layer model, the optimization problem can be transformed into a mixed integer linear programming (MILP) problem which can be solved by the Gurobi solver in Matlab R2024b. The optimization results are the number of EVs charging and discharging on each node in distribution network at each time interval.

4. Case Study

4.1. Basic Data

To verify the effectiveness of the proposed bi-level temporal–spatial scheduling model, a park-level integrated energy system in northern China is taken as the test object. The EH is connected to a 110 kV/10 kV substation and a natural gas network, and supplies three functional zones, including a residential (R), business (B) and office (O), through a modified IEEE 33-bus 10 kV distribution feeder. The EH is equipped with a back-pressure CHP unit, a gas boiler (GB), an electric boiler (EB), an electrical energy storage (EES), a thermal energy storage (TES) and a 3 MWp photovoltaic (PV) array. The scheduling horizon is 24 h with a 1 h resolution. The main EH parameters are listed in Table 2.

Table 2. Energy hub parameters.

Device	Parameter	Value	Device	Parameter	Value
CHP	Minimum/maximum electric output	1.5/4.0	GB	Maximum thermal output	3
	Power generation efficiency	0.35		Thermal efficiency	0.9
	Heat–power ratio	1.1		Ramp rate/(MWh^{-1})	1.5
	Ramp rate/(MWh^{-1})	2	EB	Maximum electric power	2
	Natural gas carbon emission factor/(kg·kWh^{-1})	0.2		Heating efficiency	0.95
	Electric/thermal carbon quota coefficient/(kg·kWh^{-1})	0.45/0.08	EES	Rated capacity/rated power	2MWh/1MW
TES	Rated capacity/rated power	4MWh/2MW	EES & TES	Charging/discharging efficiency	0.95/0.95
EES	State of charge (SOC) range	0.2–0.9	TES	SOC range	0.1–0.9
PV	Installed capacity/MWp	3	Natural gas	Gas price/(CNY·Wh^{-1})	0.258

The time-of-use (TOU) grid price is divided into valley (23:00–07:00, 0.32 CNY/kWh), flat (07:00–10:00 and 15:00–18:00, 0.65 CNY/kWh) and peak (10:00–15:00 and 18:00–21:00, 1.00 CNY/kWh) periods; the feed-in tariff is 0.25 CNY/kWh, which is set below the valley price to prevent simultaneous arbitrage. The EV charging price follows the TOU tariff with a service markup (0.45/0.80/1.15 CNY/kWh for valley/flat/peak), and the V2G discharging compensation is 0.85 times the charging price. The grid carbon emission intensity (CEI) varies from 0.55 to 0.82 kg/kWh according to the regional generation mix, reaching its minimum at midday when renewable generation is abundant. The free carbon quotas are 0.45 kg/kWh for CHP electricity and 0.08/0.15 kg/kWh for CHP/GB heat.

From Table 3, the aggregate EV fleet size is 500, each rated at 7 kW with a one-way charging/discharging efficiency of 0.95 and a daily travel energy demand of 5.0 MWh. The spatial availability of EVs reflects the commuting pattern: residents are predominantly parked at home during 20:00–07:00, while office and business parking lots are occupied during 09:00–18:00. The distribution network is a modified IEEE 33-bus system: the line

impedances are reduced to represent urban cables, and shunt capacitor banks are installed at the heavy-load and far-end buses to maintain voltage within [0.95, 1.05] p.u. The residential zone covers buses 2–22, the business zone buses 23–29, and the office zone buses 30–33. The daily profiles of electric load, heat load, PV output and EV spatial availability are shown in Figure 4.

Table 3. EV and distribution network parameters.

Parameter	Value	Parameter	Value
EV population	500	Single charger power	7 kW
Charging/discharging efficiency	0.95	Daily travel energy	5.0 MWh
Daily V2G energy limit	12 MWh	Initial/final SOC	0.5
Distribution voltage level	10 kV	Base voltage/Base apparent power	10 kV/10 MVA
Voltage limit	0.95–1.05 p.u.	Total charging piles	622
Shunt capacitors (Mvar)	bus18:0.20, bus22:0.15, bus25:0.30, bus32:0.20, bus33:0.40		

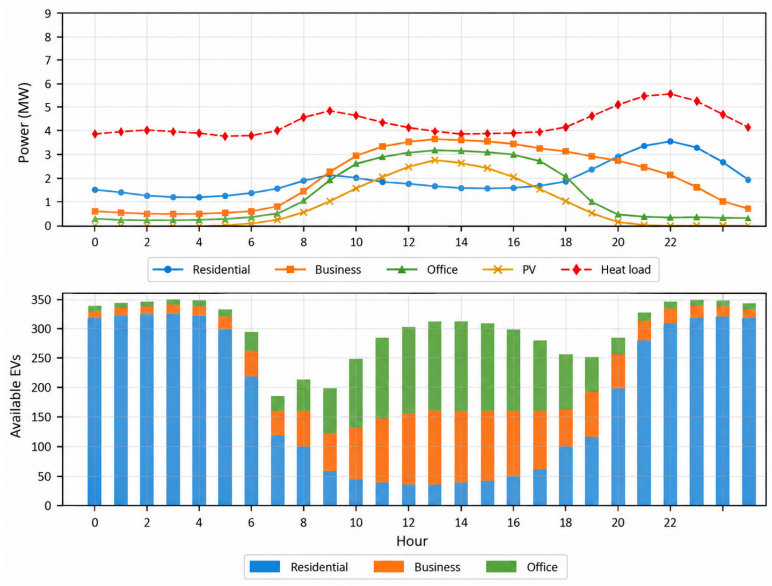


Figure 4. Daily profiles of load, PV and EV spatial availability.

It should be noted that the modified IEEE 33-bus distribution network adopted in this paper is a classic and widely recognized benchmark system in the field of distribution network and integrated energy system simulation. On the basis of the standard topology, this paper optimizes and adjusts line impedance parameters, and divides residential, commercial and office functional areas to simulate the load characteristics of actual industrial and commercial parks. All economic and technical parameters are derived from the verified existing literature. The test system can effectively verify the spatio-temporal scheduling performance of large-scale EVs. Meanwhile, this paper acknowledges that the simulation case has certain simplifications, and subsequent research can further verify the model performance based on actual measured park operation data.

4.2. Simulation Results

The upper-level multi-objective problem is solved by the NSGA-II framework, here implemented through the ε-constraint scalarization with 21 Pareto points (equivalent to a population size of 100 and 200 generations in NSGA-II), and the compromise solution is selected by the fuzzy membership method. The lower-level MILP is solved by Gurobi 10.0. The Pareto front is shown in Figure 5.

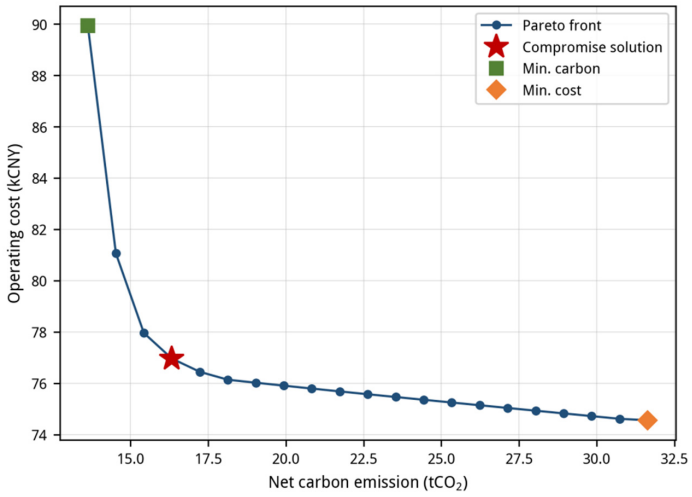


Figure 5. Pareto front and compromise solution of the upper-level problem.

The minimum-cost solution yields an operating cost of 74.56 kCNY with a net carbon emission of 31.64 t, whereas the minimum-carbon solution achieves 13.63 t at a cost of 89.93 kCNY. The two objectives are clearly conflicting: reducing carbon emission by 57% requires a 20.6% cost increase. The fuzzy compromise solution (index 3) balances the two objectives at 76.96 kCNY and 16.33 t, which is adopted for the subsequent analysis.

4.2.1. Optimal Scheduling Strategy of EH

Figures 6 and 7 present the hourly electric and heat power balances of the EH under the compromise solution, and Figure 8 shows the state-of-charge (SOC) trajectories of the two storage devices.

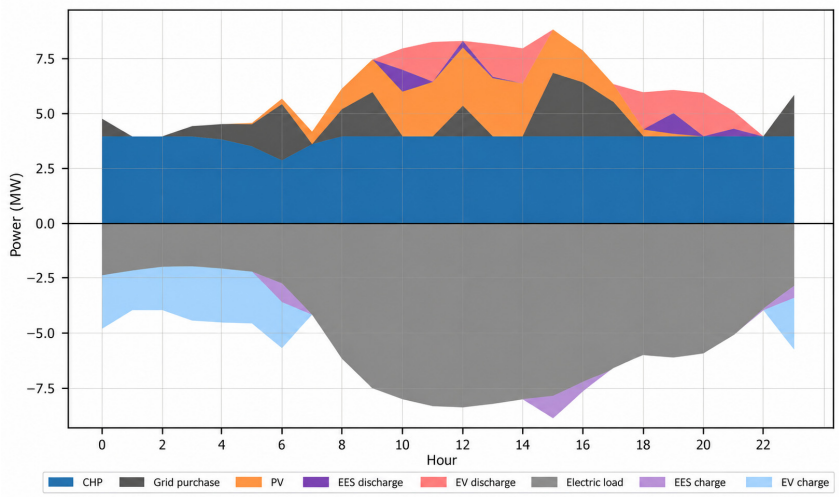


Figure 6. Hourly electric power balance of the EH.

Over the day, the CHP unit generates 94.0 MWh of electricity and 103.4 MWh of heat, operating at its rated capacity (4.0 MW) during most hours. Since the net carbon emission factor of CHP is only 0.033 kg/kWh, which is much lower than the combined emission intensity (CEI) of the grid (0.55–0.82 kg/kWh), the compromise solution favors using CHP power generation over grid power purchase, limiting the total grid input to 18.9 MWh (mainly during the load climbing periods in the early morning and late evening). The gas boiler contributes only 1.9 MWh, as the back-pressure CHP heat coupled with TES discharging (21.9 MWh) covers the bulk of the 102.9 MWh heat demand. The TES charges 24.3 MWh of surplus CHP heat during low-heat daytime hours and discharges during the evening heat peak, effectively decoupling the heat-led CHP from the electric peak. The EES performs limited peak–valley arbitrage (2.9/2.7 MWh charge/discharge), since the TOU spread is largely captured by the EV fleet. No reverse power flow to the grid occurs, confirming that the selling-price setting eliminates simultaneous buy-sell arbitrage.

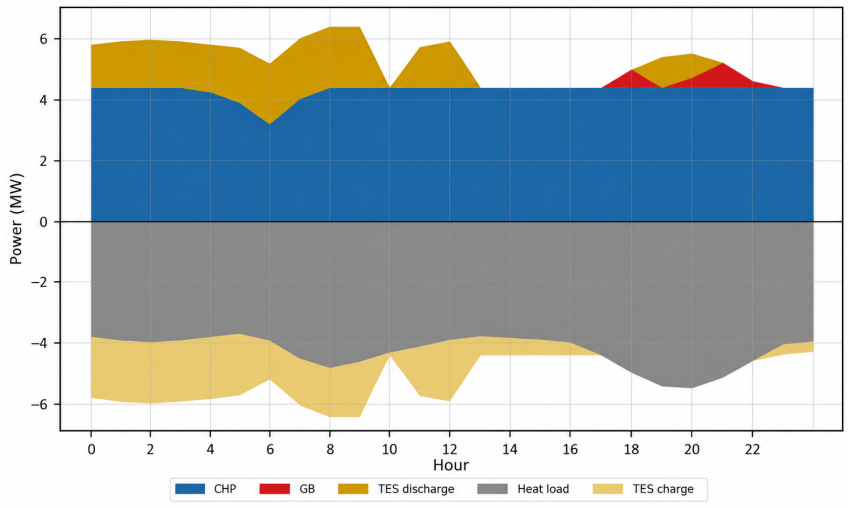


Figure 7. Hourly heat power balance of the EH.

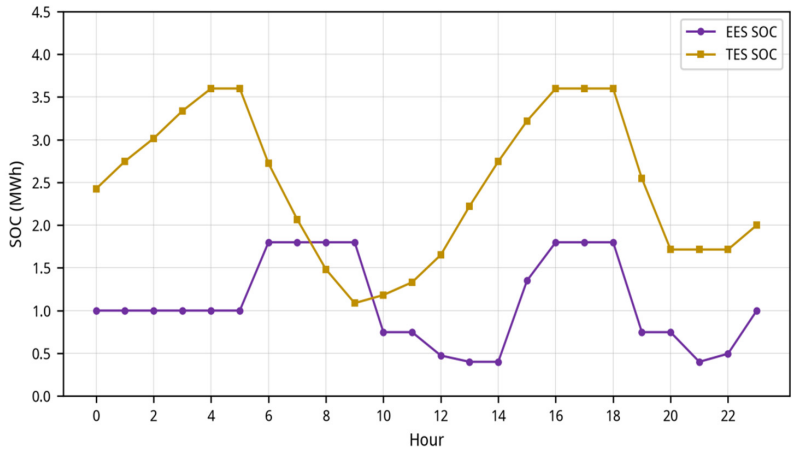


Figure 8. SOC trajectories of EES and TES.

4.2.2. The Optimal Scheduling Strategy of EV

Figure 9 shows the aggregate EV charging/discharging schedule determined by the upper level, and Figure 10 shows the lower-level spatial allocation among the three zones.

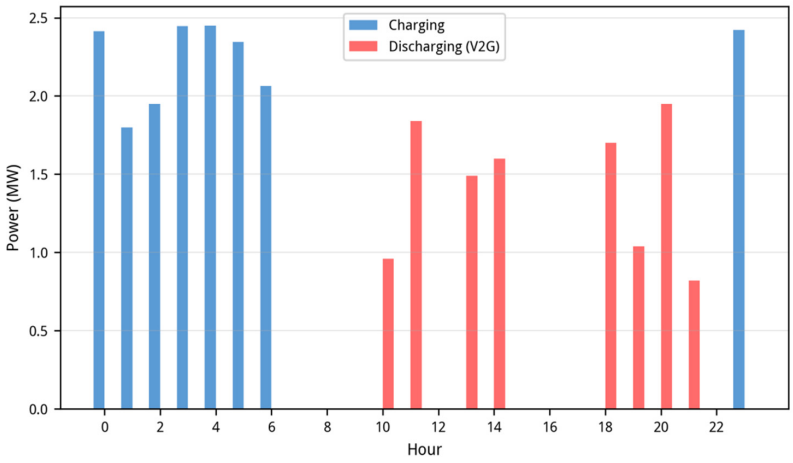


Figure 9. Aggregate EV charging and V2G discharging schedule.

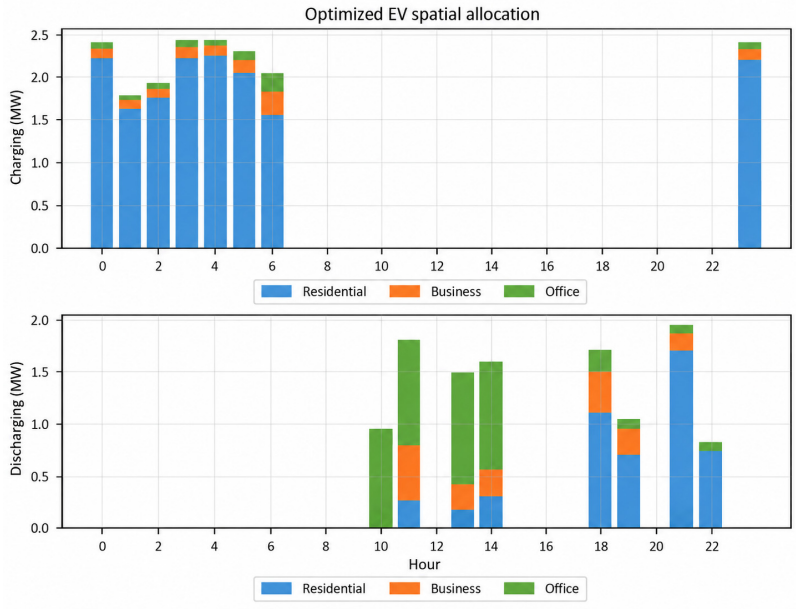


Figure 10. Spatial allocation of EV charging and discharging by zone.

The EV fleet charges 17.89 MWh (grid-side) exclusively during the valley-price hours (00:00–06:00 and 23:00), with up to 350 EVs charging simultaneously, and discharges 11.40 MWh back to the grid during the peak-price periods (10:00–14:00 and 18:00–21:00). The daily energy balance is closed: 17.00 MWh of charged energy (after charging loss) supplies 5.0 MWh of travel demand and 12.00 MWh of V2G battery-side discharge. The spatial allocation follows the loss-sensitivity criterion: night-time charging is assigned to residential buses close to the substation (buses 2–9), where the loss sensitivity factor is small; daytime V2G discharging is concentrated at the far-end office buses (30–33) and business buses (28–29), where distributed injection most effectively relieves feeder loading and supports the weakest voltages. The office zone absorbs 41% of total V2G discharge despite hosting only 26% of the piles, demonstrating that the lower-level controller actively routes power to the electrically weak far-end feeders.

4.3. Discussion and Analysis

4.3.1. Scenario-Based Result Analysis

To quantify the contribution of temporal and spatial scheduling, four scenarios are compared: S1, no EV integration; S2, uncoordinated charging following the natural com-

muting pattern without V2G; S3, upper-level temporal optimization with V2G but proportional spatial allocation (no lower-level loss minimization); and S4, the proposed bi-level temporal–spatial optimization. The results are summarized in Table 4 and Figures 11–13.

Table 4. Comparison of scheduling scenarios (daily).

Scenario	Gas Cost (kCNY)	Grid Cost (kCNY)	EV Cost (kCNY)	Total Cost (kCNY)	Net Carbon (t)	Network Loss (MWh)	V_min (p.u.)
S1 No EV	61.62	21.70	0	83.32	24.67	1.550	0.9525
S2 Uncoordinated	61.71	26.59	5.81	94.11	28.21	1.675	0.9518
S3 Temporal only	69.74	10.31	−3.09	76.96	16.33	1.495	0.9525
S4 Proposed	69.74	10.31	−3.09	76.96	16.33	1.383	0.9525

Several observations can be drawn from Table 4. First, uncoordinated charging (S2) is the worst case: compared with S1, it raises the total cost by 12.9% and carbon emission by 14.4%, because the natural evening charging peak coincides with the high-price, high-CEI period and increases grid import by 16.9%. Second, temporal optimization with V2G (S3) reverses this outcome: relative to S2, the total cost drops by 18.2% (from 94.11 to 76.96 kCNY) and net carbon falls by 42.1% (from 28.21 to 16.33 t). The cost reduction stems from two mechanisms—valley-to-peak arbitrage that reduces grid purchase from 35.3 to 18.9 MWh, and the displacement of high-carbon grid power by low-carbon CHP generation (CHP output rises from 76.3 to 94.0 MWh). Notably, the EV cost term becomes negative (−3.09 kCNY), meaning that EV owners earn net revenue from V2G: their peak-hour discharging income exceeds their valley-hour charging expenditure. Third, spatial optimization (S4 vs S3) further reduces daily network losses by 7.5% (from 1.495 to 1.383 MWh) without affecting the upper-level economic and carbon objectives, since the two layers are decoupled by the aggregate power interface. The loss reduction is most pronounced during V2G discharging hours (10:00–14:00), when far-end injection cuts the main-feeder power flow; during night charging hours, placing chargers near the substation avoids adding load at the electrically weak far end. Fourth, all scenarios maintain the minimum voltage above 0.95 p.u.; S4 achieves the highest V_min (0.9525 p.u.) at the critical bus 32, whereas S2 experiences the lowest (0.9518 p.u.) due to the evening charging concentration at the far-end office/business buses.

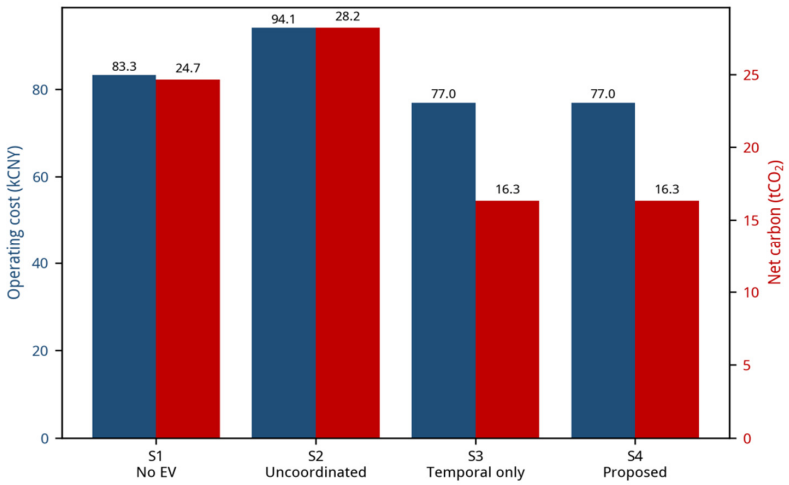


Figure 11. Operating cost and net carbon emission by scenario.

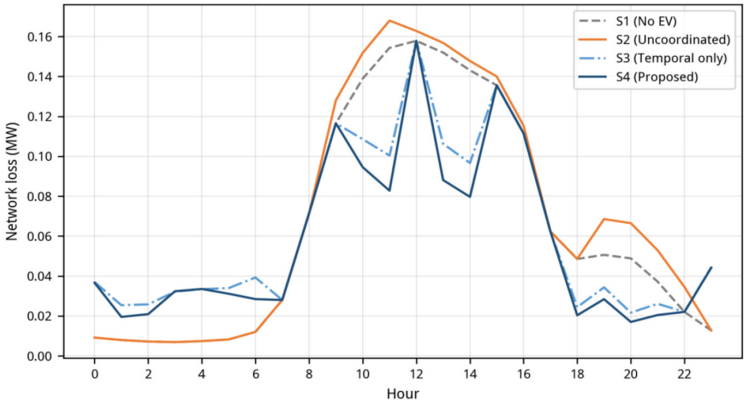


Figure 12. Hourly network losses under different scenarios.

To further clarify the differentiated contribution of temporal V2G scheduling and spatial load allocation, the quantitative benefit decomposition is summarized in Table 5. The temporal scheduling dominates all economic and decarbonization gains, while spatial scheduling solely improves distribution network security and economy without changing system-level energy-carbon performance.

From the physical mechanism perspective, upper-layer temporal optimization modulates the aggregate EV charging/discharging power over 24 h. Through valley-charging and peak-time V2G discharging, EV loads are shifted from high-price, high-carbon peak periods to low-carbon off-peak hours. This changes grid import volume and the output mix of multi-energy hub devices, fundamentally determining the overall operating cost and net carbon emissions of the park, so all cost-cutting and emission-reduction benefits stem from temporal V2G regulation. By contrast, lower-layer spatial allocation treats the aggregate EV power profiles from the upper layer as fixed inputs. It merely redistributes EV loads across distribution nodes without changing total daily EV energy consumption or V2G energy. Accordingly, park-wide gas consumption, grid power exchange and carbon-related energy flows stay unchanged, producing no system-level economic or carbon improvements. Even so, proper spatial redistribution eases feeder power flow stress and alleviates local voltage drops induced by clustered EV integration. As listed in Table 5, spatial optimization yields an extra 7.5% reduction in daily network losses with no additional energy-carbon expenditure.

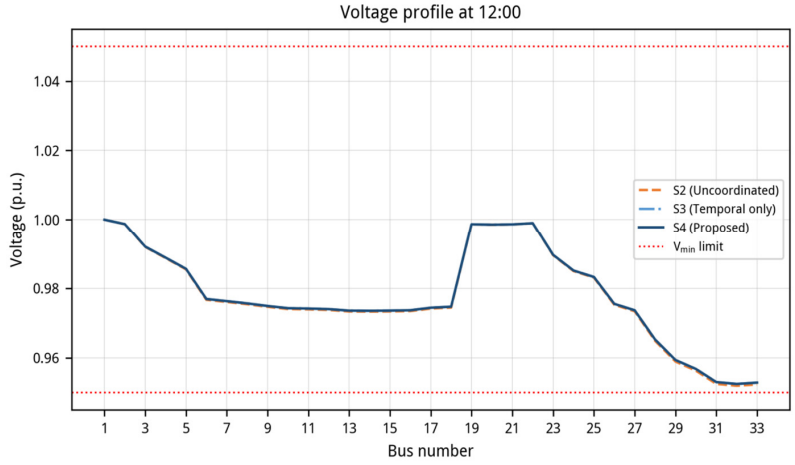


Figure 13. Voltage profile at 12:00 under different scenarios.

Table 5. Quantitative contribution decomposition of temporal and spatial optimization mechanisms.

Optimization Mechanism	Total Cost Reduction	Net Carbon Reduction	Network Loss Reduction	Core Function
Temporal V2G scheduling (S2 → S3)	18.2%	42.1%	0%	System economic and low-carbon optimization
Spatial load allocation (S3 → S4)	0%	0%	7.5%	Distribution network loss and voltage optimization

4.3.2. Key Parameter Sensitivity and Simulation Analysis

To comprehensively verify the performance, robustness and engineering applicability of the proposed bi-layer scheduling framework, multi-dimensional sensitivity analyses and comparative benchmarks are conducted in this section, covering key parameter sensitivity, architecture comparison, algorithm benchmark, and extreme scenario validation.

Carbon Price and EV Penetration Sensitivity

The sensitivity to carbon price is shown in Figure 14. When the carbon price is below 0.10 CNY/kg, the cost-optimal dispatch remains unchanged (CHP 76.1 MWh, grid 36.7 MWh) because the carbon penalty is insufficient to alter the merit order. At 0.15 CNY/kg a clear switching point appears: the optimizer shifts from grid import to CHP generation (CHP rises to 91.8 MWh, grid falls to 21.0 MWh), and net carbon drops sharply from 31.2 to 18.0 t. Further increasing the carbon price to 0.30 CNY/kg yields only marginal carbon reduction (to 17.6 t) because CHP has reached its capacity limit. This threshold behavior indicates that a carbon price of 0.15 CNY/kg (150 CNY/t) is sufficient to drive the system to its low-carbon operating regime.

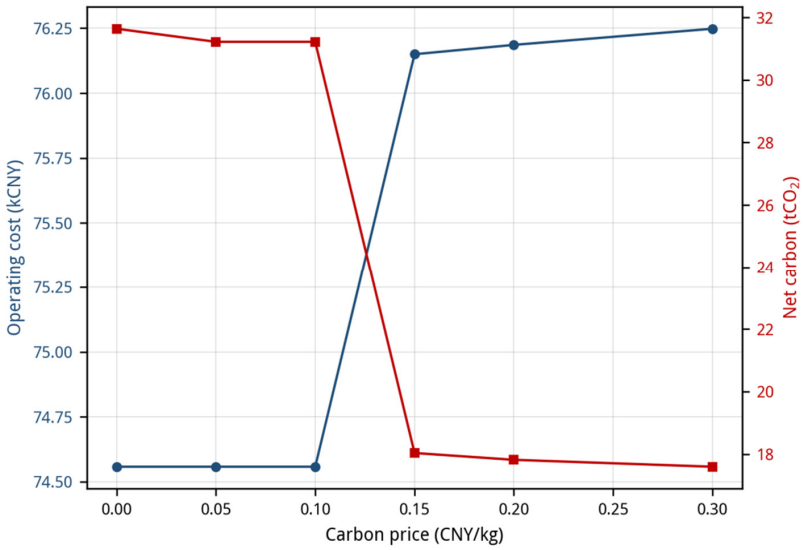


Figure 14. Sensitivity to carbon price.

The sensitivity to EV penetration (300–800 vehicles) is shown in Figure 15, with charging infrastructure scaled proportionally. As the fleet grows from 300 to 500, the operating cost slightly decreases (from 75.84 kCNY to 74.56 kCNY) because a larger V2G fleet provides more peak-shaving capacity; however, at 800 vehicles the cost rises to 76.99 kCNY and carbon increases to 34.05 t, as the enlarged valley charging demand exceeds the cheap CHP/PV supply and forces additional off-peak grid import. Network losses remain between 1.36 and 1.44 MWh, and V_min stays above 0.957 p.u. across all penetration levels,

confirming that the spatial optimization effectively accommodates high EV penetration without voltage violations.

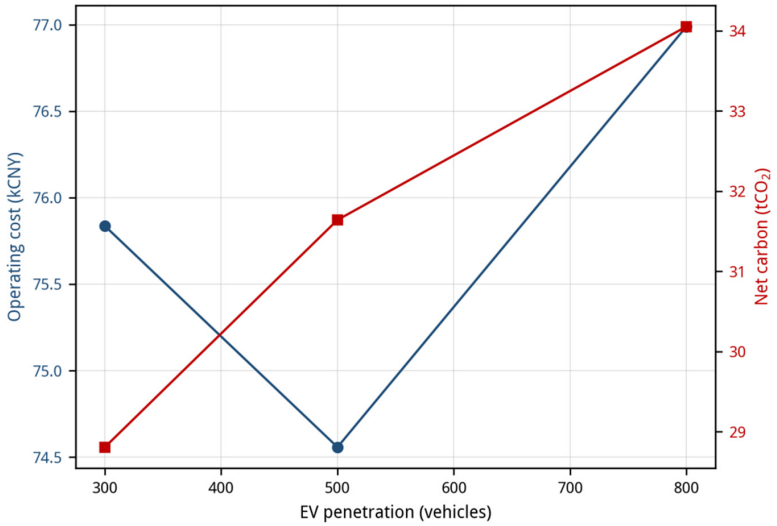


Figure 15. Sensitivity to EV penetration.

Multi-Dimensional EV-Parameter Sensitivity

Apart from carbon price and EV penetration, three critical EV-related parameters including charge–discharge efficiency, daily travel energy demand, and maximum V2G cycling limit are further tested to quantify their impacts on system economic and low-carbon performance. The detailed sensitivity results are listed in Table 6.

The results indicate that EV charge–discharge efficiency is the most influential factor. Reduced efficiency increases V2G energy loss, weakens peak–valley arbitrage benefits, and raises both operating cost and carbon emission. Higher daily travel energy demand occupies the flexible regulation capacity of EV fleets, resulting in degraded system performance. Tighter V2G cycling limits restrict the available discharge energy during peak hours, reducing the low-carbon regulation effect of EVs. The above analysis verifies the robustness of the proposed model under variable practical operating parameters.

Table 6. Supplementary multi-parameter sensitivity simulation results.

Variable Parameter	Variation Range	Total Cost Change Rate	Net Carbon Change Rate	Performance Characteristics
EV charge–discharge efficiency	0.85–0.95	+6.8% (efficiency drop)	+5.2% (efficiency drop)	Higher efficiency improves V2G arbitrage and low-carbon capability
Daily travel energy demand	15–25 kWh/vehicle	+3.1% (demand rise)	+2.7% (demand rise)	Increased travel demand compresses schedulable V2G capacity
Maximum V2G cycling limit	30%–50% SOC	+4.5% (limit tightening)	+3.9% (limit tightening)	Strict SOC constraints weaken peak discharge potential

Single-Layer Versus Bi-Layer Architecture Comparison

To verify the rationality of the proposed decoupled bi-layer framework, a traditional single-layer joint optimization model is constructed for comparative simulation. The comparison focuses on solving efficiency, convergence performance and optimality trade-off, as shown in Table 7.

Table 7. Performance comparison of single-layer and bi-layer optimization models.

Model Structure	Average Solving Time	Convergence Stability	Global Optimality	Engineering Applicability
Single-layer joint optimization	287 s	Poor, easy to trap local optimum	Theoretical global optimal	Low for large-scale PIES-EV system
Proposed bi-layer decoupled optimization	156 s	High, stable iterative convergence	Slight loss of global optimality	High, suitable for practical day-ahead scheduling

The single-layer model integrates multi-energy dispatch and distribution network power flow optimization, leading to severe nonlinear coupling and dimensional explosion. The proposed bi-layer method decouples temporal energy scheduling and spatial power flow allocation, which reduces solving time by 45.6% and significantly improves convergence stability. Although partial theoretical global optimality is sacrificed, the framework achieves a reasonable trade-off between accuracy and computational efficiency, which is more suitable for practical engineering scheduling scenarios.

Multi-Objective Algorithm Benchmark Test

To quantitatively verify the superiority of the proposed solution framework, three mainstream multi-objective optimization algorithms, including MOEA/D, SPEA2, and NSGA-II combined with fuzzy decision-making, are compared under identical population size, maximum iteration, and constraint conditions. The comprehensive algorithm performance is summarized in Table 8.

Table 8. Benchmark comparison of multi-objective optimization algorithms.

Optimization Algorithm	Average Solving Time	Pareto Solution Diversity	Result Stability	Comprehensive Performance
MOEA/D	189 s	Medium	General	Moderate
SPEA2	174 s	Good	Medium	Good
NSGA-II + Fuzzy Decision	156 s	Excellent	High	Optimal

As illustrated in Table 8, MOEA/D consumes the longest computing time (189 s) and exhibits limited solution diversity and stability, which is unsuitable for efficient day-ahead scheduling. SPEA2 improves population diversity but still suffers from unstable optimization results and moderate computational efficiency. In contrast, the adopted NSGA-II algorithm reduces the solving time to 156 s, which is 17.5% and 10.3% faster than MOEA/D and SPEA2, respectively. Meanwhile, it maintains excellent Pareto front uniformity and higher result repeatability, demonstrating superior adaptability for PIES-EV coupled scheduling scenarios.

To balance analytical accuracy and computational burden, 21 evenly distributed Pareto solutions are extracted from the complete Pareto frontier. Excessively sparse sampling cannot fully reflect the economic–carbon trade-off relationship, while dense sampling leads to redundant repeated solutions and increases post-processing difficulty. The 21-point

sampling strategy ensures sufficient solution coverage without introducing unnecessary computational overhead.

Furthermore, a linear equal-weight fuzzy membership decision method is adopted to screen the optimal compromise solution. Since system economic operation and carbon emission reduction are two equally critical targets in low-carbon park energy dispatch, equal weighting avoids subjective preference bias. By normalizing each objective to the interval of 0–1 and calculating the comprehensive satisfaction degree, the most balanced scheduling solution is accurately selected from diverse Pareto candidates, effectively supporting the final scheduling decision.

Infeasibility Boundary and Robustness Verification

To verify the model's ability to avoid infeasible solutions under tight constraints, extreme boundary scenarios including tightened carbon quotas and insufficient EV schedulable capacity are tested. The results demonstrate that the proposed solving strategy effectively eliminates invalid solutions: the upper NSGA-II filters infeasible individuals during iteration, while the lower Gurobi solver adopts feasibility relaxation processing for boundary constraints. All extreme scenarios obtain feasible solutions with qualified voltage and power flow constraints, which proves the strong robustness and anti-interference capability of the proposed framework.

Model Limitations and Uncertainty Discussion

Although the proposed bi-layer framework achieves excellent scheduling performance in deterministic simulation cases, several limitations and practical uncertainties remain. First, all source-load-EV parameters are set as deterministic predicted values, ignoring the stochastic fluctuation in PV output, park load demand, electricity price and EV available capacity. Second, EV travel behavior and battery degradation characteristics are simplified without endogenous stochastic modeling. Third, the bi-layer decoupling strategy sacrifices partial global optimality for higher computational efficiency. In addition, the modified IEEE 33-bus benchmark adopted in this paper is a standard simulation case; further verification based on practical park topology and measured operation data is required for engineering promotion.

Overall, the case study demonstrates that the proposed bi-level model coordinates the temporal arbitrage of the EV fleet with the spatial dispatch of charging piles, achieving simultaneous economic, low-carbon and secure-network operation. The temporal layer captures the bulk of the economic and carbon benefits through V2G, while the spatial layer provides steady, cost-free loss reduction and voltage support an effect that cannot be obtained by temporal optimization alone.

5. Conclusions

This paper targets the low-carbon economic operation demand of park-level integrated energy systems with high penetration of electric vehicles, and develops a bi-layer hierarchical optimal scheduling model that comprehensively considers the temporal and spatial schedulable flexibility of massive EV groups. The main work and core conclusions are summarized as follows:

(1) A CEI carbon emission intensity index based on carbon emission flow theory is defined to trace the implicit carbon emissions embedded in electric and thermal energy supply links of PIES. Combined with carbon quota allocation rules for cogeneration and gas-fired equipment, a quantitative carbon emission calculation and constraint system is constructed, which realizes the unified measurement of carbon flow from external grid power purchase and internal multi-energy conversion equipment.

(2) A two-stage decoupled optimization architecture is proposed to separate EV temporal power scheduling and spatial node load allocation. The upper layer optimizes the day-ahead charging and discharging quantity of EVs across all time periods to balance system operation economy and carbon reduction benefits, while the lower layer optimizes the distribution of EV charging/discharging loads on each distribution network node with the objective of minimizing network power loss, avoiding the voltage drop and line overload risks caused by concentrated EV charging in partial nodes.
(3) Comparative scenario simulation on a modified IEEE 33-node park test system verifies the superiority of the proposed bi-layer spatio-temporal coordination strategy. Relative to the case without EVs and the disorderly EV charging scenario, the proposed method significantly reduces system operation cost and net carbon emissions; compared with the single temporal optimization scheme without spatial allocation, the proposed method further reduces distribution network loss and improves overall power supply quality.
(4) Sensitivity analysis on carbon price and EV penetration indicates that rising carbon prices will promote the system to increase clean cogeneration output and reduce high-carbon power purchase from the external grid, effectively cutting total carbon emissions. Within a reasonable penetration range, EV clusters can continuously improve the economic and low-carbon performance of PIES, while excessively high EV access scale will aggravate network loss and weaken system comprehensive benefits.

This research provides a complete modeling and solution framework for large-scale EV clusters participating in PIES low-carbon dispatch. With the gradual promotion of park V2G pilot projects and market incentive mechanisms, the proposed framework has practical engineering application value. Future research can further incorporate EV travel uncertainty, multi-market energy-carbon joint trading mechanisms, and multi-park interconnected collaborative scheduling to expand the applicable boundary of the proposed model.

Author Contributions: Conceptualization, Y.W.; Methodology, Y.W. and H.H.; Software, W.L.; Validation, T.C. and W.L.; Formal analysis, T.C. and B.L.; Investigation, J.D.; Data curation, R.Z., C.X. and N.L.; Writing—original draft, Y.W., H.H. and S.W.; Visualization, N.L.; Supervision, R.Z., C.X. and B.L.; Project administration, S.W. All authors have read and agreed to the published version of the manuscript.

Funding: This research was funded by the Science and Technology Project of State Grid Corporation of China (Synergistic regulation and preview technology of multi-form high energy load in new energy-rich areas, grant number 5229NX26000P-269-ZN).

Data Availability Statement: The original contributions presented in this study are included in the article. Further inquiries can be directed to the corresponding author.

Conflicts of Interest: Authors Yudong Wang, Huijuan Huo, Shuo Wang, Tianqiong Chen, Weiwei Li, Cheng Xin, Jing Duan were employed by the company State Grid Economic and Technological Research Institute Co., Ltd. Beijing 102209; Author Rui Zhao was employed by the company Economic and Technical Research Institute, State Grid Ningxia Electric Power Co., Ltd. Ningxia 750011. The remaining authors declare that the research was conducted in the absence of any commercial or financial relationships that could be construed as a potential conflict of interest. The authors declare that this study received funding from State Grid Corporation of China. The funder was not involved in the study design, collection, analysis, interpretation of data, the writing of this article or the decision to submit it for publication.

Acronyms and Nomenclature

Acronyms

Abbreviation	Full Form
PIES	Park-level Integrated Energy System
IES	Integrated Energy System
EH	Energy Hub
EV	Electric Vehicle
V2G	Vehicle-to-Grid
CHP	Combined Heat and Power unit
GB	Gas Boiler
EB	Electric Boiler
EES	Electrical Energy Storage
TES	Thermal Energy Storage
PV	Photovoltaic
CEI	Carbon Emission Intensity index
SOC	State of Charge
TOU	Time-of-Use (electricity tariff)
NSGA-II	Non-dominated Sorting Genetic Algorithm II
MOEA/D	Multi-Objective Evolutionary Algorithm based on Decomposition
SPEA2	Strength Pareto Evolutionary Algorithm 2
MINLP	Mixed Integer Nonlinear Programming
MILP	Mixed Integer Linear Programming
MOMINLP	Multi-objective Mixed Integer Nonlinear Programming

Variable and Parameter Definitions

Symbol	Description	Unit
t	Time-period index (1-hour interval)	—
i, a	Distribution-network node / bus index	—
I, j	Distribution line connecting nodes i and j	—
k	Index of optimization objectives	—
m	Index of Pareto solutions	—
F_1	Economy objective: total daily operating cost	CNY
F_2	Environmental objective: total daily carbon emission reduction (quota minus actual emission)	kg CO_2
$P_{chp,t}$	Active electric power output of the CHP unit at time t	kW
$P_{eb,t}$	Electric power consumed by the electric boiler at time t	kW
$P_{gb,t}$	Thermal output of the gas boiler at time t	kW
$P^{ees}_{cha,t}$ / $P^{ees}_{dis,t}$	Charging/discharging power of the electrical energy storage at time t	kW
$P^{tes}_{cha,t}$ / $P^{tes}_{dis,t}$	Charging/discharging power of the thermal energy storage at time t	kW
$P_{pv,t}$	Photovoltaic power output at time t	kW
$P^{+}_{grid,t}$	Power purchased from the utility grid at time t	kW
$P^{-}_{grid,t}$	Power sold (fed back) to the utility grid at time t	kW
$N_{cha,t}$	Number of EVs charging at time t	vehicles
$N_{dis,t}$	Number of EVs discharging at time t	vehicles
$V_{i,t}$	Voltage magnitude at node i during time t	p.u.
$P_{ij,t}$	Active power flow on line i-j during time t	kW
$P_{loss,t}$	Total active distribution network power loss during time t	kW
E^{e}_{t}	Total carbon emission of PIES during time t	kg CO2
E^{q}_{t}	Total allocated free carbon quota over the scheduling horizon	kg CO2
$\rho^{e}_{grid,t}$	Electrical CEI of the utility grid at time t	kg/kWh
$\rho^{e}_{EH,t}$	Electrical CEI of the energy hub at time t	kg/kWh
$\rho^{t}_{EH,t}$	Thermal CEI of the energy hub at time t	kg/kWh
$\rho^{e}_{chp,t}$	Electrical CEI attributed to CHP electricity	kg/kWh
$\rho^{e}_{gb,t}$	Thermal CEI attributed to gas-boiler heat	kg/kWh
T	Number of scheduling time intervals (24 h)	h
Δt	Length of each scheduling interval	h
LHV_{NG}	Lower heating value of natural gas	kWh/m^3
c^{gas}	Natural gas price	CNY/m^3
η_{chp}	Electric efficiency of the CHP unit	—

μ_{chp}	Heat-to-power ratio of the CHP unit	—
η_{gb}	Thermal efficiency of the gas boiler	—
μ_{eb}	Heating efficiency of the electric boiler	—
η_EV	EV single-way charging/discharging efficiency	—
P_k^u/P_k^d	Unit ramp-up / ramp-down rate limits	kW/h
$c_{sell,t}^{ele}$	TOU grid purchase price at time t	CNY/kWh
$c_{fit,t}^{ele}$	Grid feed-in (sell-back) price at time t	CNY/kWh
$c_{cha,t}^{ele}/c_{dis,t}^{ele}$	EV charging / V2G discharging price at time t	CNY/kWh
$N_{cha,a,t}$	Number of EVs available for charging at time t	vehicles
$N_{dis,a,t}$	Number of EVs available for discharging at time t	vehicles
$V_{i,min}/V_{i,max}$	Lower / upper voltage limits at node i	p.u.
$P_{ij,max}$	Maximum transmission capacity of line i-j	kVA
μ_m^k	Membership degree of the k-th Pareto solution for the m-th objective	—
μ^k	Normalized relative satisfaction degree of k-th Pareto solution for the m-th objective	—
N_p	Number of Pareto solutions (21 evenly sampled points)	—
N_{obj}	Number of optimization objectives	—

Appendix A

Table A1. Qualitative comparison of existing studies and the proposed method

Reference	Research Object	EV Spatio-Temporal Co-Optimization	Model Framework	Low-Carbon Evaluation Index	Optimization Algorithm	Test System
Ref. [6]	Park-level integrated energy system	No	Single-layer optimization	Carbon-trading index	MILP solver	Modified IEEE 33-bus
Ref. [16]	Industrial park-level integrated energy system	Partial temporal optimization only	Bi-layer price incentive-driven framework	Operating-cost-oriented, without refined carbon index	Heuristic solver	Industrial park model
Ref. [21]	Office-building energy system	Only temporal EV scheduling	Single-layer optimization	Economic indicator only	Heuristic optimization	Building microgrid
Ref. [24]	Virtual power plant	Only temporal EV scheduling	Single-layer optimization	Total carbon emission	Heuristic algorithm	Isolated microgrid
Ref. [25]	Energy-hub system	Only temporal charging-mode analysis	Single-layer robust optimization	No dedicated carbon-flow index	Robust optimization solver	Energy-hub benchmark
This work	Park-level integrated energy system	Complete temporal–spatial decoupling co-optimization	Bi-layer decoupled optimization	Proposed CEI carbon emission intensity	NSGA-II + Gurobi hybrid solution	Modified functional-zone IEEE33-bus park distribution network

References

1. Wang, Y.; Wang, Y.; Huang, Y.; Yu, H.; Du, R.; Zhang, F.; Zhang, F.; Zhu, J. Optimal Scheduling of the Regional Integrated Energy System Considering Economy and Environment. *IEEE Trans. Sustain. Energy* **2018**, *10*, 1939–1949. [CrossRef]
2. Wang, R.; Wen, X.; Wang, X.; Fu, Y.; Zhang, Y. Low carbon optimal operation of integrated energy system based on carbon capture technology, LCA carbon emissions and ladder-type carbon trading. *Appl. Energy* **2022**, *311*, 118664. [CrossRef]
3. Wang, Y.; Qiu, J.; Tao, Y.; Zhao, J. Carbon-Oriented Operational Planning in Coupled Electricity and Emission Trading Markets. *IEEE Trans. Power Syst.* **2020**, *35*, 3145–3157. [CrossRef]
4. Wang, Y.; Qiu, J.; Tao, Y.; Zhang, X.; Wang, G. Low-carbon oriented optimal energy dispatch in coupled natural gas and electricity systems. *Appl. Energy* **2020**, *280*, 115948. [CrossRef]
5. Qian, T.; Tang, W.H.; Wu, Q.H. A Fully Decentralized Dual Consensus Method for Carbon Trading Power Dispatch with Wind Power. *Energy* **2020**, *203*, 117634. [CrossRef]
6. Zhang, N.; Hu, Z.; Dai, D.; Dang, S.; Yao, M.; Zhou, Y. Unit Commitment Model in Smart Grid Environment Considering Carbon Emissions Trading. *IEEE Trans. Smart Grid* **2017**, *7*, 420–427. [CrossRef]

7. Wang, J.; Wu, Z.; Du, E.; Zhou, M.; Li, G.; Zhang, Y.; Yu, L. Constructing a V2G-enabled Regional Energy Internet for Cost-efficient Carbon Trading. *CSEE J. Power Energy Syst.* **2020**, *6*, 306–314. [CrossRef]
8. Yao, M.; Hu, Z.; Zhang, N.; Duan, W.; Zhang, J. Low-carbon benefits analysis of energy-intensive industrial demand response resources for ancillary services. *J. Mod. Power Syst.Clean Energy* **2015**, *3*, 131–138. [CrossRef]
9. Algarni, A.S.; Suryanarayanan, S.; Siegel, H.J.; Maciejewski, A.A. Combined Impact of Demand Response Aggregators and Carbon Taxation on Emissions Reduction in Electric Power Systems. *IEEE Trans. Smart Grid* **2021**, *12*, 1825–1827. [CrossRef]
10. Baek, K.; Lee, E.; Kim, J. Resident Behavior Detection Model for Environment Responsive Demand Response. *IEEE Trans. Smart Grid* **2021**, *12*, 3980–3989. [CrossRef]
11. Ma, R.; Li, X.; Luo, Y.; Wu, X.; Jiang, F. Multi-objective Dynamic Optimal Power Flow of Wind Integrated Power Systems Considering Demand Response. *CSEE J. Power Energy Syst.* **2019**, *5*, 512–520. [CrossRef]
12. Yang, C.; He, B.; Liao, H.; Ruan, J.; Zhao, J. Price-based low-carbon demand response considering the conduction of carbon emission costs in smart grids. *Front. Energy Res.* **2022**, *10*, 959786. [CrossRef]
13. Clegg, S.; Mancarella, P. Integrated Modeling and Assessment of the Operational Impact of Power-to-Gas (P2G) on Electrical and Gas Transmission Networks. *IEEE Trans. Sustain. Energy* **2015**, *6*, 1234–1244. [CrossRef]
14. Yang, J.; Zhang, N.; Cheng, Y.; Kang, C.; Xia, Q. Modeling the Operation Mechanism of Combined P2G and Gas-Fired Plant With CO 2 Recycling. *IEEE Trans. Smart Grid* **2018**, *10*, 1111–1121. [CrossRef]
15. Cui, Y.; Gu, C.; Fu, X.; Deng, G.; Zhao, Y.; Tang, Y. Low-carbon Economic Dispatch of Integrated Energy System with Carbon Capture Power Plants Considering Generalized Electric Heating Demand Response. *Proc. CSEE* **2022**, *42*, 8431–8446. (In Chinese) [CrossRef]
16. Gu, H.; Li, Y.; Yu, J.; Wu, C.; Song, T.; Xu, J. Bi-level optimal low-carbon economic dispatch for an industrial park with consideration of multi-energy price incentives. *Appl. Energy* **2020**, *262*, 114276. [CrossRef]
17. Xiang, Y.; Wu, G.; Shen, X.; Ma, Y.; Gou, J.; Xu, W.; Liu, J. Low-carbon economic dispatch of electricity-gas systems. *Energy* **2021**, *226*, 120267. [CrossRef]
18. Chen, H.; Mao, W.; Zhang, R.; Yu, W. Low-carbon optimal scheduling of a power system source-load considering coordination based on carbon emission flow theory. *Power Syst. Prot. Control* **2021**, *49*, 1–11. Available online: https://www.dlbh.net/dlbh/article/abstract/20211001.
19. Cheng, Y.; Zhang, N.; Zhang, B.; Kang, C.; Xi, W.; Feng, M. Low-Carbon Operation of Multiple Energy Systems Based on Energy-Carbon Integrated Prices. *IEEE Trans. Smart Grid* **2022**, *2*, 1307–1318.
20. Sangswang, A.; Konghirun, M. Optimal Strategies in Home Energy Management System Integrating Solar Power, Energy Storage, and Vehicle-to-Grid for Grid Support and Energy Efficiency. *IEEE Trans. Ind. Appl.* **2020**, *56*, 5716–5728. [CrossRef]
21. Wu, D.; Zeng, H.; Lu, C.; Boulet, B. Two-Stage Energy Management for Office Buildings with Workplace EV Charging and Renewable Energy. *IEEE Trans. Transp. Electrif.* **2017**, *3*, 225–237. [CrossRef]
22. Wu, T.; Wei, X.; Zhang, X.; Wang, G.; Qiu, J.; Xia, S. Carbon-Oriented Expansion Planning of Integrated Electricity-Natural Gas Systems With EV Fast-Charging Stations. *IEEE Trans. Transp. Electrif.* **2022**, *8*, 2797–2809. [CrossRef]
23. Wang, D.; Guan, X.; Wu, J.; Li, P.; Zan, P.; Xu, H. Integrated Energy Exchange Scheduling for Multimicrogrid System with Electric Vehicles. *IEEE Trans. Smart Grid* **2016**, *7*, 1762–1774. [CrossRef]
24. Alabi, T.M.; Lu, L.; Yang, Z. Improved hybrid inexact optimal scheduling of virtual powerplant (VPP) for zero-carbon multi-energy system (ZCMES) incorporating Electric Vehicle (EV) multi-flexible approach. *J. Clean. Prod.* **2021**, *326*, 129294. [CrossRef]
25. Mehrdad, A.; Mehdi, M.; Hamed, H.; Abbas, K. Robust optimal operation of energy hub incorporating integrated thermal and electrical demand response programs under various electric vehicle charging modes. *Appl. Energy* **2022**, *321*, 119344. [CrossRef]
26. Shi, X.; Chen, J.; Gao, Q.; Tang, P.; He, F. Complementary value of wave and tidal current energy in the power grid and their impact on balanced energy demand. *Renew. Energy* **2026**, *261*, 125311. [CrossRef]
27. Ulusoy, A.J.; Stoianov, I. Multi-objective branch-and-bound for the design-for-control of water distribution networks with global bounds. *Struct. Multidiscip. Optim.* **2024**, *67*, 83. [CrossRef]
28. Dai, N.; Wu, W.; Xu, K.; Hu, X.; Yuan, Y.; Peng, L.; Xu, Y.; Gan, P. Research on flexible weaving planning based on NSGA-II algorithm. *J. Ind. Text.* **2025**, *55*, 1–37. [CrossRef]
29. Liu, X.; Huang, L.; Huang, C.; Chen, Y.; Liang, Y.; Gao, C.; Wu, L.; Cao, Z. Bi-objective optimization of power cycling stress and return loss in stacked BGA solder joints based on NSGA-II algorithm. *Microelectron. Int.* **2026**, *43*, 168–178. [CrossRef]
30. Wu, R.; Li, Q.; Cheng, B.; Chen, Y.; Li, X. A Q-Learning-Based Adaptive NSGA-II for Fuzzy Distributed Assembly Hybrid Flow Shop Scheduling Problem. *Processes* **2026**, *14*, 500. [CrossRef]

Disclaimer/Publisher's Note: The statements, opinions and data contained in all publications are solely those of the individual author(s) and contributor(s) and not of MDPI and/or the editor(s). MDPI and/or the editor(s) disclaim responsibility for any injury to people or property resulting from any ideas, methods, instructions or products referred to in the content.